A CLIMATOLOGY OF MELT ONSET/OFFSET OVER SNOW AND LAND ICE IN THE NORTHERN HEMISPHERE FROM PASSIVE MICROWAVE REMOTE SENSING

1. ABSTRACT

We assessed melting trends in the Arctic over the 1979 – 2015 period by means of passive microwave 37 GHz vertically polarized brightness temperature. Melt is detected using a dynamic (both in space and in time) version of the DAV algorithm, introduced by *Tedesco et al., 2009*, which makes use of the difference between the daytime and the nighttime brightness temperature (T_b) signal (DAV or Diurnal Amplitude Variation). As liquid water appears in the snowpack, the T_b signal shows an abrupt increase and the DAV signal (computed as the running difference between daytime and nighttime T_b) reaches the highest values, indicating that melting season has started. Computing single year Melt Onset Date (MOD), Melt End Date (MED) and Melting Season Length (MSL) maps for the 1979-2015 period and interpolating them, let us to find melting trends for the Arctic as the slope of the of the linear regression fitting single year – maps. On the average, 90% level statistically significant results suggest that melting, in the 1979 – 2015 period, has been starting and finishing earlier and the length of the melting season has been shortening as well.

2. INTRODUCTION

The aim of this work, developed at the Lamont Doherty Earth Observatory (Columbia University in the City of New York) under the supervision of prof. Roberto Ranzi and prof. Marco Tedesco, consists in assessing melting trends in the Arctic, for the period 1979-2015, by means of passive microwave 37 GHz vertically polarized brightness temperature. Monitoring snow related processes, thus studying how the climate system is responding to present day forcings is of primary importance because it allows us to have data useful for water resources evaluation, management and control of watershed, analysis of long-term trends and assessment of human activities potential effects on the natural resources (*Ranzi et al., 1999*). As a consequence, I decided to focus my thesis on the assessment of melting trends, evaluating, in this way, how the cryosphere is reacting to natural and anthropogenic forcings. Melting of snow can be described through spaceborne passive microwave remote sensing, making use of spaceborne microwave brightness temperature time-series, $T_b s$, available from 1979. At frequencies greater than 10 GHz, a rapid increase in emissivity occurs as a result of a small amount (~1-2%) of liquid water within the snowpack, causing the T_b to increase for wet snow. At the time of melting, the daytime T_b signal shows high value due to the presence of wet snow, while, during the night, it drops considerably beneath the winter condition, causing large DAVs, which become footprints of melt. This is easy to notice by looking at *Figures 1a, 1b, 1c*, referring to a snow covered pixel of the Arctic: in presence of melting the T_b time series shows an abrupt increase and large DAVs are registered (between days 80 and 130). DAVs remain large as the T_b keeps fluctuating at the beginning of the melting season, then it drops down to relatively small values since no significant differences between nighttime and daytime T_b s are registered (from day 131 on).

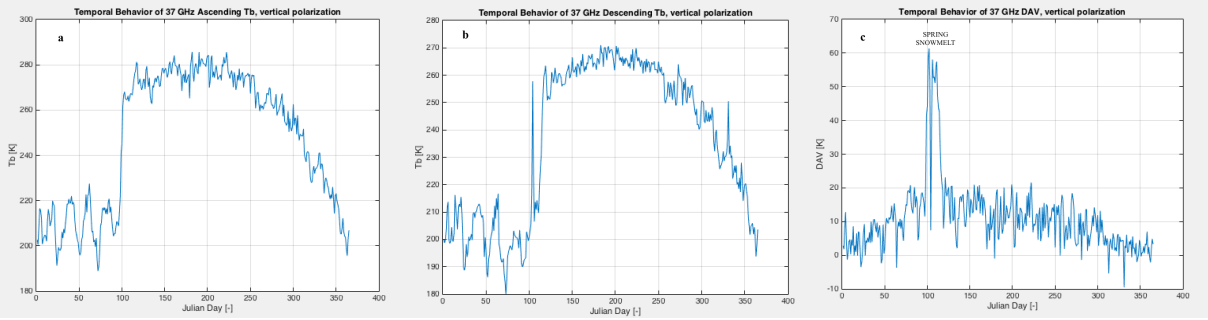

Figure 1: Typical 37 GHz vertically polarized annual T_b time series, ascending passes (a) and descending passes (b); typical 37 GHz vertically polarized annual DAV signal.

3. DATA

Data consist of vertically polarized T_b at Ka band (ν between 27 and 40 GHz) measured by three different passive sensors: the Scanning Multichannel Microwave Radiometer or SMMR (from 1978 to 1987), the Special Sensor Microwave/Imager or SSM/I (from 1987 to date) and the NASA/NASDA's Advanced Microwave Scanning Radiometer for EOS or AMSR-E (2002-2011). We decided to deal with 36.5 and 37 GHz data in order to exploit the ability of such frequencies signal in differentiating between dry and wet snow (*Macelloni et al., 2001*).

As a result, it was necessary to perform cross-platform calibration and it consisted in using linear regression to identify relationship between brightness temperatures from both sensors (*e.g. Dai et al., 2015).* Sensors involved have different spatial, temporal and radiometric characteristics (*Table 1*): this affects brightness temperature continuity and consistency and it may lead to inaccuracy or to errors when determining various surface parameters, as well as when determining long term melting trends. Globally, by considering both ascending and descending observations, dataset consisted in about 30000 images and they were supplied by the National Snow and Ice Data Center (NSIDC), as shown in *Table 2*.

SENSORS	SMMR	SSM/I (F08)	SSM/I (F11)	SSM/I (F13)	SSM/I (F17)	AMSR-E
Platform	NIMBUS-7	DMSP-F08	DMSP-F11	DMSP-F13	DMSP-F17	EOS-Aqua
Time series	1978.10.26-1987.8.20	1987.7.9-1991.12.30	1991.12.3-1995.9.30	1995.5.3-2009.4.1	2008.1.1-present	2002.6.19-2011.9.27
Frequency at Ka band [GHz]	37	37	37	37	37	36.5
IFOV (lenght [km] * width [km])	27*18	37*28	37*28	37*28	37*28	14*8
Polarization	V&H	V&H	V&H	V&H	V&H	V&H
Viewing Angle [°]	50.2	53.1	53.1	53.1	53.1	55
Swath Width [km]	780	1400	1400	1400	1400	1445
Ascending Overpass time (local time)	12:00 PM	5.30-7.30 PM	5.30-7.30 PM	5.30-7.30 PM	5.30-7.30 PM	12.30-2.30 PM
Descending Overpass time (local time)	0.00 AM	7.30-9.00 AM	7.30-9.00 AM	7.30-9.00 AM	7.30-9.00 AM	2.30-4.30 AM

Table 1: Passive microwave sensors table of features.

SENSOR	1-Oct-79	9-Jul-87	20-Aug-87	3-Dec-91	30-Dec-91	3-May-95	30-Sep-95	19-Jun-02	1-Jan-08	1-Apr-09	27-Jun-11	30-Sep-15	Ascending Data [-]	Descending Data [-]	Total number of Data
SMMR													1392	1464	2856
SSM/I (F08)													1523	1481	3004
SSM/I (F11)													1358	1447	2805
SSM/I (F13)													4839	4736	9575
SSM/I (F17)													2453	2453	4906
AMSR-E													3260	3260	6520
												TOTAL	14825	14841	29666

Table 2: Consistency table for dataset.

4. METHOD

T_b records, organized in hydrological years, were processed to get MOD, as well as MED and MSL Pan-Arctic maps through the D-DAV approach, an update of the well known DAV method.

The basic idea behind it is that melt onset is characterized by melting during daytime and refreezing during nighttime. According to this approach, histograms of T_b swath data are plotted versus a fitted bimodal probability distribution, which is supposed to model such histograms. Brightness temperatures are measured in both dry and wet conditions: dry snow observations are assumed to belong to the left normal distribution (termed LND) and wet snow data are assumed to belong to its right normal distribution (RND). So wet snow is assumed to occur once a certain T_b threshold (called T_c) has been overcome and when a certain DAV threshold (called DAV_C) has been overcome as well. Such thresholds are spatially and temporally dynamic and this let the fitting procedure to be as suitable as possible; in particular, for each pixel and for all the hydrological years, its T_b threshold, called T_c is computed from the parameters of the T_b bimodal distribution fitting the histograms of the T_b swath data, while its DAV threshold, called DAV_C is computed as the mean of the DAV values for the months of January and February, plus a fixed value of 10 K. So, according to this algorithm, MOD (MED) occurs as the first (last) day in which one of the following conditions is verified:

- $DAV_i > DAV_c \cap T_{b,i} \geq T_c$ being $T_{b,i}$ either an ascending or a descending brightness temperature and DAV_i the Diurnal Amplitude Variation for a given day, computed as the difference between the daytime and the nighttime T_b values.
- $T_{b,i}^a \geq {T_c}^a \cap T_{b,i}^d \geq {T_c}^d$ being $T_{b,i}^a$ and $T_{b,i}^d$ a, respectively, ascending and descending brightness temperature and ${T_c}^a$, ${T_c}^d$ the related thresholds.

T_b thresholds are computed as $T_{1,2} = \frac{-B \pm \sqrt{|(B^2 - 4AC)|}}{2A}$, being $A = s_1^2 - s_2^2$, $B = 2(m_1 s_2^2 - m_2 s_1^2)$ and $C = m_2^2 s_1^2 - m_1^2 s_2^2 + 2 s_1^2 s_2^2 * \ln\left(s_2 * \frac{p}{s_1} * (1-p)\right)$, both for ascending and descending data. In particular, P it's a mixture of two Gaussian G probability distribution functions and it makes a total of 5 parameters: the mean and the standard deviation of each distribution $(m_i; s_i)$and the p parameter, which represents the percentage of dry pixels. The value of $T_{1,2}$ falling in the $[m_1;\ m_2]$ interval is the so-called T_c threshold, beyond which melting is supposed to begin. If no one of the two values falls in such range, the threshold will be set equal to 255 K as a default, according to other previous studies, like *Tedesco et al., 2006*. Clearly, MSL, for each year, is got as the number of days included between MOD and MED. 90% level statistically significant 1979-2015 Pan-Arctic melting trends in terms of MOD, MED and MSL were determined as the slope of the linear regression fitting data, excluding pixels which did not satisfy any of the conditions set for melting.

5. RESULTS AND DISCUSSION

Single year ascending and descending T_b threshold maps were got for all the hydrological years included in the 1979 – 2015 time range and showed results consistent with latitude: the smaller the latitude, the higher the T_bs and, accordingly, the higher its threshold (*Figures 2a, 2b*). This occurred since, for each pixel, the computation of its $T_b$thresholds is dynamic and it is based upon the the probabilistic fitting of real swath data (*Figure 2c*): ${T_c}^a$and ${T_c}^d$ depend on the parameters of the bimodal distribution fitting the frequency histograms. The histograms pattern shows that there are few intermediate T_b values in the time series: as the temperature is increasing, the emissivity

increases more with only small increase in moisture. So, T_b threshold can be found in this minimum range of values.

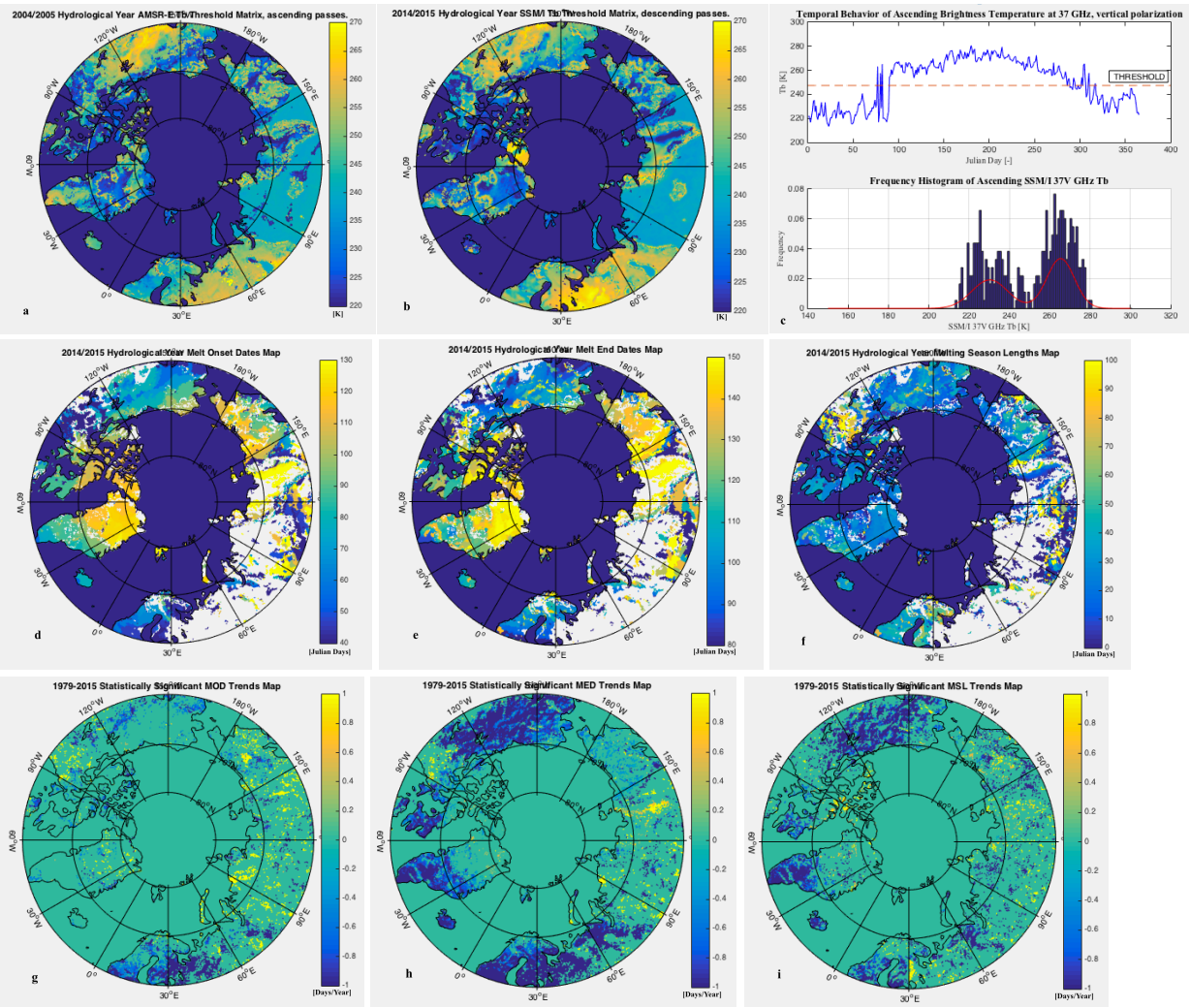

Figure 2: 2004/2005 Hydrological Year AMSR-E ascending T_b thresholds map (a); 2014/2015 Hydrological Year SSM/I descending T_b thresholds map (b); Single pixel annual ascending T_b time series and frequency histogram (c); 2014/2015 Hydrological Year MODs Map (d); MEDs Map (e); MSLs Map (f);1979-2015 90% level statistically significant MOD trends map (g), MED trends map (h), MSL trends map (i).

Annual MOD, MED and MSL maps were obtained for all the hydrological years under investigation and they show that melting follows a trend which is consistent with the latitude.
On the average, pixels located at progressively larger latitudes resulted to melt progressively later. As a consequence, MOD (*Figure 2d*) and MED (*Figure 2e*) resulted to be larger (on an absolute scale) by moving northward; of course, the differences in terms of Julian days between MED and MOD decreased by moving northward. The melting conditions set at the beginning of this work resulted to be satisfied for a number of days decreasing with increasing latitude. Melting season followed a trend proportional to latitude, as well: the greater the latitude, the shorter the melting season (*Figure 2f*). This means that pixels at the highest latitudes showed the smallest melting season lengths. White-painted pixels did not respect any of the two conditions set for melting, thus

they were not involved into the algorithm. This was probably due to the presence of high forest cover, which plays a central role during the retrieval *(e.g. Santi et al., 2012)* and to the differences in the overpass times between sensors (*Table 1*). Single year MOD, MED and MSL maps were, then, interpolated in order to find melting trends expressed in terms of days/year. 90% level statistically significant melting trends were obtained by computing the slope of the linear regression fitting single year – maps. *Figure 2* also shows maps of D-DAV derived melting trends (*2g, 2h* and *2i*) over the 1979-2015 period: according to the D-DAV algorithm derived model, on the average, over the past 36 years melting has been starting (finishing) $\sim 0.35\ \frac{days}{year}$ ($\sim 1\ \frac{days}{year}$) earlier and the length of the melting season has been shortening by $\sim 0.9\ \frac{days}{year}$. The most negative trends occurred in North America, as well as in the South of Greenland and in Europe. Russian pixels resulted to have either less negative results or not to be involved in the algorithm, as well as the northern region of Greenland. On the other hand, the great majority of positive trends occurred in the Russian area and few of them were also present in Canada.

6. CONCLUDING REMARKS

- Melt onset detected as a 'jump' in T_b from passive microwave radiometers exhibits latitudinal trends which are consistent with the climatology of the cryosphere;
- The date of melt onset, on the average, has been occurring earlier as well as the date of the melt end and the melting season length. These results are in line with the ones of other previous similar studies like *Tedesco et al., 2009 and Bliss & Anderson, 2014*.
- 36 consecutive hydrological years were investigated, thus results got can be considered as possible proofs of climate change, being the time-interval larger than 30 years.
- A comparison of satellite-derived information with in situ measurements would be useful for a verification of the methodology and the results we obtained.

7. REFERENCES

Bliss, A. C., & Anderson, M. R. (2014). Snowmelt onset over Arctic sea ice from passive microwave satellite data: 1979-2012. *The Cryosphere*, *8*(6), 2089–2100.

Dai, L., Che, T., & Ding, Y. (2015). Inter-Calibrating SMMR, SSM/I and SSMI/S Data to Improve the Consistency of Snow-Depth Products in China. *Remote Sensing*, *7*(6), 7212–7230.

Macelloni, G., Paloscia, S., Pampaloni, P., Tedesco, M., & Sites, A. T. T. (2001). Microwave Emission From Dry Snow : A Comparison of Experimental and Model Results, *39*(12), 2649–2656.

Ranzi, R., Grossi, G., & Bacchi, B. (1999). Ten years of monitoring areal snowpack in the Southern Alps using NOAA-AVHRR imagery , ground measurements and hydrological data Abstract :, *2095*(May 1998).

Santi, E., Pettinato, S., Paloscia, S., Pampaloni, P., Macelloni, G., & Brogioni, M. (2012). An algorithm for generating soil moisture and snow depth maps from microwave spaceborne radiometers : HydroAlgo, 3659–3676.

Tedesco, M., Kim, E. J., England, A. W., Roo, R. D. De, & Hardy, J. P. (2006). Brightness Temperatures of Snow Melting/Refreezing Cycles: Observations and Modeling Using a Multilayer Dense Medium Theory-Based Model. *IEEE Transactions on Geoscience and Remote Sensing*. JOUR .

Tedesco, M., Brodzik, M., Armstrong, R., Savoie, M., & Ramage, J. (2009). Pan arctic terrestrial snowmelt trends (1979-2008) from spaceborne passive microwave data and correlation with the Arctic Oscillation. *Geophysical Research Letters*, *36*(21), 1–6.